Iterative Reconstruction for Differential Phase Contrast Imaging

Thomas Köhler, Bernhard Brendel, and Ewald Roessl
Philips Technologie GmbH, Innovative Technologies, Research Laboratories, D–22335 Hamburg, Germany

Purpose: The purpose of this work is to combine two areas of active research in tomographic x-ray imaging. The first one is the use of iterative reconstruction techniques. The second one is differential phase contrast imaging (DPCI).

Method: We derive an SPS type maximum likelihood (ML) reconstruction algorithm with regularization for DPCI. Forward and back-projection are implemented using spherically symmetric basis functions (blobs) and differential footprints, thus completely avoiding the need for numerical differentiation throughout the reconstruction process. The method is applied to the problem of reconstruction of an object from sparsely sampled projection.

Results: The results show that the proposed method can handle the sparely sampled data efficiently. In particular no streak artifacts are visible which are present images obtained by filtered back-projection (FBP).

Conclusion: Iterative reconstruction algorithms have a wide spectrum of proven advantages in the area of conventional computed tomography. The present work describes for the first time, how a matched forward and back-projection can be implemented for DPCI, which is furthermore free of any heuristics. The newly developed ML reconstruction algorithm for DPCI shows that for the case of sparsely sampled projection data, an improvement in image quality is obtained that is qualitatively comparable to a corresponding situation in conventional x-ray imaging. Based on the proposed operators for forward and back-projection, a large variety of iterative reconstruction algorithms is thus made available for DPCI.

Keywords: iterative reconstruction, differential phase contrast imaging, compressed sensing, blobs

I. INTRODUCTION

Iterative reconstruction in general and statistical iterative reconstruction in particular is currently one of the hot topics in tomographic x-ray imaging. The objectives and applications of iterative reconstruction algorithms include dose reduction[1,2], sparse sampling[3,4], and limited angle tomography[5,6].

Another new trend in X-ray imaging is phase contrast imaging. This became recently feasible even with a conventional x-ray tube by using a Talbot-Lau interferometer[7–9] and is known as differential phase contrast imaging (DPCI). This technique shows excellent soft-tissue contrast[10–12] that would likely add diagnostic value if applicable to human imaging.

Barely any work has been published so far on a combination of DPCI and iterative reconstruction. In fact, we are aware only of the work by Qi et al.[13]. In their work, a total variation minimization algorithm was adopted to the field of DPCI. The implementation by Qi et al. requires empirical weighting factors since in their implementation, the derivative is implemented as a weighted sum of projections through the image differentiated along the two major axes.

In the present work, we propose a new way to handle the differential nature of the projection data by using blobs as basis functions in image domain and appropriate footprints, which is an elegant and natural way to implement differential forward projection.

II. METHOD

The basic prerequisites of an iterative reconstruction algorithm are a discrete representation of the image and a discrete implementation of a forward projection operator. A single projection value is parameterized in 2D by the projection angle θ and the distance ϱ of the ray to the origin. Let δ be a vector that represents the image, i. e., the real part of the refractive index of the object, and P_θ be a conventional projection operator with the projection direction θ. The measured differential data d_θ of a projection taken at direction θ correspond to the first derivative of $P_\theta\delta$ with respect to ϱ:

$$d_\theta = \partial_\varrho P_\theta \delta \,. \tag{1}$$

Qi et al. implemented the differentiation by exchanging differentiation and projection and splitting the differentiation with respect to ϱ into a weighted sum of differentiations along the two major axes of the coordinate system. Here, we include the differentiation directly into a forward operator A.

Since we want to avoid a numerical implementation of the derivatives, we rather adapt the idea of using blobs to represent the image. Specifically, we use the well-known Kaiser-Bessel functions as proposed by Lewitt[14]

$$b_{m,a,\alpha}(r) = \begin{cases} \frac{\left(1-(r/a)^2\right)^{m/2} I_m\left(\alpha\sqrt{1-(r/a)^2}\right)}{I_m(\alpha)} & \text{for } r \le a \\ 0 & \text{for } r > a \end{cases} \tag{2}$$

where r is the distance from the center of the blob, I_m denotes the modified Bessel function of order m, a is the

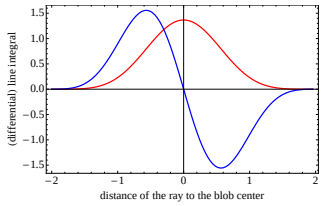

FIG. 1: Footprint of a Kaiser-Bessel blob and its derivative for $a = 2$, $m = 2$, and $\alpha = 10.826$.

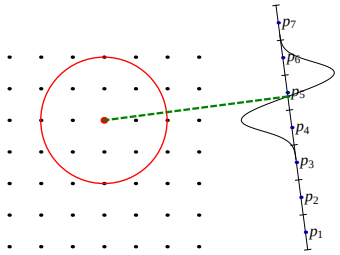

FIG. 2: Illustration of forward projection using blobs. A sample blob (thick red dot in the image grid) has a support as indicated by the red circle. The contribution of this blob to the differential projection is obtained by forward projection of the blob center to the detector (dashed green line) in order to determine the relative position of the differential footprint to the detector and to sample the pre-tabulated differential footprint at the detector pixel centers p_i.

radial dimension of the blob, and α is a taper parameter controlling the blob shape. The beauty of this approach is that the projection of an image element does not depend on the projection direction and that this projection can be calculated analytically. In an implementation of a forward projection using blobs as basis functions, this projection of the basis function, the so-called footprint, is stored in a lookup table. A finite detector pixel size is accounted for by a convolution of the footprint with the pixel size. Now turning to the problem of differential data, we note that differentiation is a linear operator and thus instead of calculating a derivative of the entire projection, we can equivalently calculate the derivative of the conventional contribution of each blob independently. This can be conveniently implemented by using the derivative of the conventional footprint, which can also be calculated analytically. Fig. 1 shows the conventional footprint of a 2D Kaiser-Bessel blob and the differential footprint to be used for DPCI.

Fig. 2 illustrates how to calculate the elements a_{ij} of the system matrix A.

In DPCI, the differential data d are generated by a fit of a cosine function to a couple of intensity measurements[8]. Therefore, it is reasonable to assume Gaussian noise on these data. The variance of the data d_i is denoted σ_i^2. Then the log-likelihood function (omitting constant terms) is

$$L(\delta) = -\frac{1}{2}\sum_i \frac{1}{\sigma_i^2}\left(d_i - [A\delta]_i\right)^2 . \tag{3}$$

Next, we aim at deriving an SPS-type algorithm[15] for the problem of maximization of the log-likelihood function. Using the definition $h_i(l) = -(d_i - l)^2/(2\sigma_i^2)$, the log-likelihood function can be written as

$$L = \sum_i h_i([A\delta]_i). \tag{4}$$

We denote the current image estimate as $\delta^{(n)}$ and the resulting current estimate for the differential line integrals as $d^{(n)}$ with the relation

$$d_i^{(n)} = \sum_j a_{ij}\delta_j^{(n)} . \tag{5}$$

Now we can write the log-likelihood function as

$$L = \sum_i h_i\left(\sum_j a_{ij}\left(\delta_j - \delta_j^{(n)}\right) + d_i^{(n)}\right) . \tag{6}$$

Since h is concave, we can apply Jensen's inequality for any set of weights $\alpha_{ij} \geq 0$ with $\sum_j \alpha_{ij} = 1$, leading to

$$L = \sum_i h_i\left(\sum_j \alpha_{ij}\left(\frac{a_{ij}}{\alpha_{ij}}\left(\delta_j - \delta_j^{(n)}\right) + d_i^{(n)}\right)\right) \tag{7}$$

$$\geq \sum_i\sum_j \alpha_{ij} h_i\left(\frac{a_{ij}}{\alpha_{ij}}\left(\delta_j - \delta_j^{(n)}\right) + d_i^{(n)}\right) , \tag{8}$$

which is a separable function in the unknown image elements δ_j. Applying the Newton-Raphson method leads to the iteration function

$$\delta_j^{(n+1)} = \delta_j^{(n)} + \frac{\sum_i a_{ij}\frac{1}{\sigma_i^2}(d_i - d_i^{(n)})}{\sum_i \frac{a_{ij}^2}{\alpha_{ij}}\frac{1}{\sigma_i^2}} . \tag{9}$$

For our algorithm we chose

$$\alpha_{ij} = |a_{ij}| / \sum_j |a_{ij}| , \tag{10}$$

where in comparison to the standard SPS algorithm[15] the absolute values of the elements a_{ij} are used in order to meet the condition of $\alpha_{ij} \geq 0$ since these elements are no longer non-negative.

Regularization can be added to the algorithm in the usual way since the total cost function $\Psi(\delta)$ to maximize is simply the sum of the log-likelihood and a roughness penalty $-\beta R(\delta)$

$$\Psi(\delta) = L(\delta) - \beta R(\delta) \tag{11}$$

where β is the regularization parameter. The roughness penalty is written in the form

$$R(\delta) = \sum_j \sum_{k\in\mathcal{N}_j} w_{jk}\psi(\delta_j - \delta_k) \tag{12}$$

where $\mathcal{N}_j$ is the set of all neighbor grid points of the grid point j, ψ is a convex potential function, and w_{jk} are weights, which can be used, e. g., to account for the geometrical distance of the grid points j and k.

Adding the regularization and inserting Eq. (10) into Eq. (9) leads to the update equation of the regularized SPS for DPCI

$$\delta_j^{(n+1)} = \delta_j^{(n)} + \frac{\sum_i \frac{a_{ij}}{\sigma_i^2}(d_i - d_i^{(n)}) - \beta\sum_{k\in\mathcal{N}_j} w_{jk}\psi'(\delta_j - \delta_k)}{\sum_i \frac{|a_{ij}|}{\sigma_i^2}\sum_j |a_{ij}| - \beta\sum_{k\in\mathcal{N}_j} w_{jk}\psi''(\delta_j - \delta_k)} . \tag{13}$$

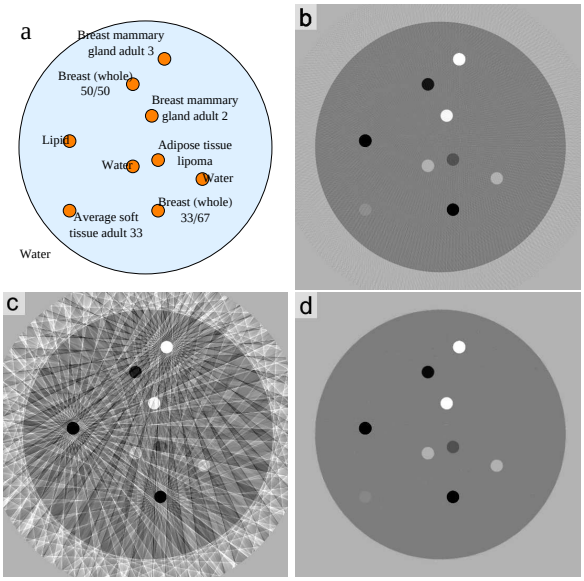

FIG. 3: a: Phantom used for simulations. The background material is breast mammary adult 1. Material definitions are taken from[17]; b: FBP reconstruction from 180 projections; c: FBP reconstruction from 20 projection; d: ML reconstruction from 20 projections.

III. RESULTS

Fig. 3 shows in the top left the mathematical phantom used in the study. Details about the simulation are given in[16]. The diameter of the object is 110 mm. A parallel beam short scan sinogram with 180 projections was simulated at 25 keV at the ninth fractional Talbot distance. The projection size was 1024 columns and the reconstruction was performed on a 512^2 grid.

Fig. 3 shows additionally reconstructed images using filtered back-projection (FBP) using 180 projections and results obtained by using only 20 projections reconstructed with FBP and the proposed algorithm with Huber regularization. While the FBP results from the undersampled data shows severe streak artifacts, the ML reconstruction still recovers the phantom quite well.

IV. SUMMARY

We presented an elegant way to set up a forward projection operator for DPCI using blobs and differential footprints that avoids any numerical differentiation and heuristic weighting in iterative reconstruction as described in former work by Qi et al.[13]. Our concept can be easily extended to a divergent beam geometry by considering the magnification. It can also easily be extended to 3D cone-beam imaging by using the 2D footprint of the 3D blob which is differentiated in one direction only. Finally, it can be used together with any optimization algorithm for the likelihood function.

We further derived an SPS-type ML reconstruction algorithm with regularization for DPCI. Initial results obtained with an edge-preserving regularization results in efficient streak reduction if applied to sparsely sampled data and thus demonstrate the validity of our approach.

[1] J.-B. Thibault, K. D. Sauer, C. A. Bouman, and J. Hsieh, "A three-dimensional statistical approach to improved image quality for multislice helical CT," Med. Phys. **34**, 4526–4544 (2007).

[2] J. Wang, T. Li, and Y. L. Xing, "Iterative image reconstruction for CBCT using edge-preserving prior," Med. Phys. **36**, 252–260 (2009).

[3] J. Tang, B. E. Nett, and G.-H. Chen, "Performance comparison between total variation (TV)-based compressed sensing and statistical iterative reconstruction algorithms," Phys. Med. Biol. **54**, 5781–5804 (2009).

[4] E. Y. Sidky and X. Pan, "Image reconstruction in circular cone-beam computed tomography by constrained, total-variation minimization," Phys. Med. Biol. **53**, 4777–4807 (2008).

[5] T. Wu, A. Stewart, M. Stanton, T. McCauley, W. Phillips, D. B. Kopans, R. H. Moore, J. W. Eberhard, B. Opsahl-Ong, L. Niklason, and M. B. Williams, "Tomographic mammography using a limited number of low-dose cone-beam projection images," Med. Phys. **30**, 365–380 (2003).

[6] E. Y. Sidky, X. Pan, I. S. Reiser, R. M. Nishikawa, R. H. Moore, and D. B. Kopans, "Enhanced imaging of microcalcifications in digital breast tomosynthesis through improved image-reconstruction algorithms," Med. Phys. **36**, 4920–4932 (2009).

[7] A. Momose, S. Kawamoto, I. Koyama, Y. Hamaishi, K. Takai, and Y. Suzuki, "Demonstration of X-ray Talbot interferometry," Jpn. J. Appl. Phys. **42**, L866–L868 (2003).

[8] T. Weitkamp, A. Diaz, C. David, F. Pfeiffer, M. Stampanoni, P. Cloetens, and E. Ziegler, "X-ray phase imaging with a grating interferometer," Opt. Express **13**, 6296–6304 (2005).

[9] F. Pfeiffer, C. Kottler, O. Bunk, and C. David, "Hard x-ray phase tomography with low-brilliance sources," Phys. Rev. Lett. **98**, 108105 (2007).

[10] F. Pfeiffer, O. Bunk, C. David, M. Bech, G. L. Duc, A. Bravin, and P. Cloetens, "High-resolution brain tumor visualization using three-dimensional x-ray phase contrast tomography," Phys. Med. Biol. **52**, 6923–6930 (2007).

[11] T. Weitkamp, C. David, O. Bunk, J. Bruder, P. Cloetens, and F. Pfeiffer, "X-ray phase radiography and tomography of soft tissue using grating interferometry," European J. of Radiology **68**, S13–S17 (2008).

[12] G. Schulz, T. Weitkamp, I. Zanette, F. Pfeiffer, F. Beckmann, C. David, S. Rutishauser, E. Reznikova, and B. Müller, "High-resolution tomographic imaging of a human cerebellum: comparison of absorption and grating-based phase contrast," J. R. Soc. Interface **7**, 1665–1676 (2010).

[13] Z. Qi, J. Zambelli, N. Bevins, and G.-H. Chen, "A novel method to reduce data acquisition time in differential phase contrast computed tomography using compressed sensing," Proc. SPIE Med. Imag. Conf. **7258**, 72584A (2009).

[14] R. M. Lewitt, "Multidimensional digital image representations using generalized Kaiser-Bessel window functions," J. Opt. Soc. Am. A **7**, 1834–1846 (1990).

[15] J. A. Fessler, "Statistical image reconstruction methods for transmission tomography," in "Handbook of Medical Imaging, Vol. 2," edited by M. Sonka and J. M. Fitzpatrick, chap. 1 (SPIE Press, Bellingham, WA, 2000), pp. 1–70.

[16] T. Koehler, K. J. Engel, and E. Roessl, "Noise properties of grating based x-ray phase contrast computed tomography," Med. Phys. **38** (2011).

[17] "Photon, electron, proton, and neutron interaction data for body tissues. ICRU report 46," International Commission on Radiation Units and Measurements, Bethesda, MD (1992).